Research Square

Preprints are preliminary reports that have not undergone peer review.
They should not be considered conclusive, used to inform clinical practice,
or referenced by the media as validated information.

TABLNet: Trustworthy Adaptive Broad Learning Network for Physical-Layer Device Authenticationin Intelligent IoT Networks

Xinyu xiang

8250811197@njfu.edu.cn

Xianyu Chen
Jinwen Liao
Dan Qin
Yi Zhang

Research Article

Keywords:

Posted Date: November 9th, 2026

DOI: https://doi.org/10.21203/rs.3.rs-11123003/v1

License: This work is licensed under a Creative Commons Attribution 4.0 International License.
Read Full License

Additional Declarations: No competing interests reported.

TABLNet: Trustworthy Adaptive Broad Learning Network for Physical-Layer Device Authentication in Intelligent IoT Networks

Abstract

Securing the expanding internet of things (IoT) ecosystem demands lightweight authentication mechanisms compatible with hardware-constrained edge endpoints. Specific emitter identification (SEI) exploits manufacturing-induced radio frequency (RF) fingerprints to verify device identity at the physical layer, circumventing the overhead of upper-layer cryptographic schemes. Nevertheless, contemporary deep generative architectures employed for automated RF fingerprint synthesis impose prohibitive computational demands that hinder their deployment on resource-limited platforms. In this paper, a trustworthy adaptive broad learning network (TABLNet) framework is proposed to overcome these limitations. Unlike deep hierarchical models, TABLNet adopts a laterally expandable flat architecture wherein raw signal samples are projected onto generative feature nodes directly connected to the decision layer. Weight optimization relies on pseudoinverse computation rather than iterative backpropagation, thereby suppressing gradient instability and substantially curtailing training duration. Moreover, an autonomous node expansion mechanism dynamically calibrates the network width, eliminating manual hyperparameter search. Comprehensive experiments on two hardware-captured RF datasets demonstrate that TABLNet achieves competitive or superior classification accuracy while delivering an order-of-magnitude reduction in training latency compared with prevailing deep learning baselines.

Keywords: Physical-layer security, specific emitter identification, broad learning system, IoT network security, edge intelligence

1 Introduction

The rapid proliferation of intelligent IoT devices—including smart home gateways, wearable health monitors, and industrial edge controllers—has intensified the demand for robust yet resource-efficient device authentication [1–3]. Traditional upper-layer security measures such as asymmetric key exchange and certificate-based encryption incur considerable computational and energy costs that tax battery-powered endpoints

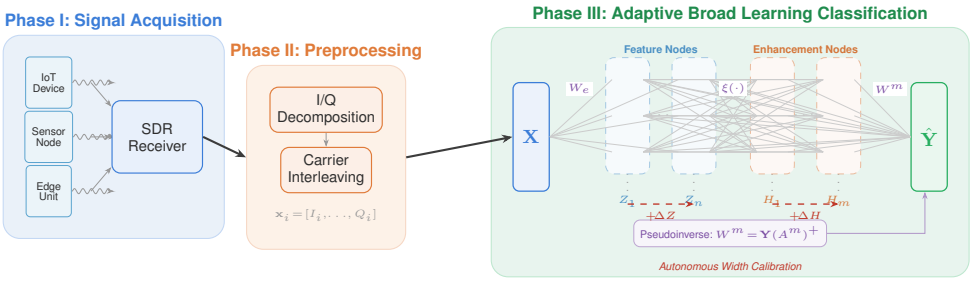


Fig. 1 Overall architecture of the proposed TABLNet framework. Phase I captures raw RF emissions from heterogeneous IoT transmitters via a software-defined radio receiver. Phase II transforms complex-valued I/Q samples into real-valued feature vectors through carrier interleaving. Phase III performs emitter classification via the flat-topology adaptive broad learning network, where feature node groups $Z_1, \ldots, Z_n$ and enhancement node groups $H_1, \ldots, H_m$ are jointly connected to the output $\hat{\mathbf{Y}}$, with terminal weights W^m derived by Moore-Penrose pseudoinverse computation. Dashed arrows indicate the autonomous width calibration mechanism.

[4, 5]. As the attack surface of IoT networks continues to expand, lightweight authentication alternatives operating below the protocol stack have attracted growing research attention [6–9].

Specific emitter identification (SEI) constitutes a promising physical-layer strategy that authenticates transmitters by exploiting radio frequency fingerprints (RFF)—subtle signal distortions arising from inherent manufacturing imperfections in transmitter hardware [10–12]. Conventional RFF extraction pipelines distinguish between transient signal features generated during power-on/off transitions and steady-state features embedded within the modulated payload. Classical approaches rely on handcrafted transformations, such as nonlinear component decomposition [13], Hilbert-based spectral analysis [14], and pulse-mode classification [15, 16]. The dependence on expert domain knowledge constrains the adaptability of these methods to the diverse, high-dimensional hardware characteristics of modern IoT transmitters [17, 18].

Deep learning has enabled end-to-end automated RFF representation learning, obviating manual feature engineering [19–25]. Architectures spanning convolutional neural networks, generative adversarial frameworks, and complex-valued networks have exhibited strong identification performance. However, such models typically depend on deep stacked layers, extensive hyperparameter spaces, and iterative gradient-based optimization, incurring high computational latency and susceptibility to gradient pathologies. Although model compression strategies like knowledge distillation [26] and structured pruning [27] can shrink parameter counts, they do not resolve the fundamental computational bottleneck inherent to backpropagation-centric training.

To surmount these constraints, a trustworthy adaptive broad learning network (TABLNet) framework is introduced [28, 29]. Departing from deep hierarchical topologies, TABLNet employs a flat network structure in which generative capacity is expanded laterally through additional feature and enhancement nodes. Terminal weights are determined via the Moore-Penrose pseudoinverse, supplanting iterative

gradient descent with a closed-form algebraic solution and thereby eliminating backpropagation overhead. An autonomous width calibration strategy further automates structural optimization, adapting the network scale to data complexity without manual intervention.

The principal contributions are threefold:

1. A flat-topology TABLNet framework is proposed for physical-layer emitter authentication on resource-constrained IoT platforms, leveraging pseudoinverse-based weight derivation to bypass backpropagation.
2. An autonomous node expansion protocol is designed to dynamically adjust the network width according to incoming signal complexity, enabling rapid on-device training and deployment.
3. Extensive experiments on two real-world RF signal datasets validate that TABLNet achieves competitive identification accuracy while reducing training time by over an order of magnitude relative to state-of-the-art deep learning methods.

The rest of this paper is organized as follows. Section 2 presents the proposed TABLNet framework. Section 2I reports the experimental results. Section 4 concludes this paper.

2 Proposed TABLNet Framework

The architectural design of the trustworthy adaptive broad learning network (TABLNet) framework and its computational core—the adaptive broad learning (ABL) network—are described in this section. The end-to-end workflow, depicted in Fig. 1, encompasses three operational stages: radio signal capture by edge-deployed sensors, specialized preprocessing for data alignment, and RF fingerprint extraction together with classification through the ABL network [2, 19, 30].

2.1 Signal Preprocessing

In typical IoT communication environments, radio emissions are captured in in-phase and quadrature (I/Q) format [24]. Each digitized symbol consists of a real component I and an imaginary component Q, the latter representing a 90-degree phase rotation of the former. The complex-valued symbol sequence encodes phase-dependent interactions between the two channels [9, 24]. To satisfy the real-valued input requirement of the broad learning architecture, each complex sample is converted into a concatenated real-valued vector through carrier interleaving:

$$\mathbf{x}_i = [I_i(1), I_i(2), \ldots, I_i(k), Q_i(1), Q_i(2), \ldots, Q_i(k)] \tag{1}$$

where $\mathbf{x}_i$ denotes the resulting real-valued representation and k indicates the number of symbols per acquisition window. This concatenation retains both amplitude and phase information necessary for subsequent RF fingerprint synthesis.

2.2 Adaptive Broad Learning Network

The broad learning infrastructure is augmented with a dynamic structural adaptation mechanism. The baseline topology is first analyzed, followed by the derivation of an incremental expansion scheme and an autonomous width calibration policy [28, 29].

2.2.1 Network Topology

In contrast to deep architectures that propagate information through multiple stacked layers, the ABL adopts a flat, resource-efficient topology composed of feature nodes, enhancement nodes, and a linear output layer (Fig. 1) [28]. Given an input matrix $\mathbf{X}$ containing preprocessed I/Q telemetry, the network produces a classification output $\mathbf{Y} \in \mathbb{R}^{N \times K}$, where N is the sample count and K is the number of device categories. The i-th feature node group Z_i is generated through a nonlinear projection governed by learned weights W_{ei} and biases β_{ei}. A sigmoid activation ensures high-fidelity feature synthesis, while a sparse autoencoder regularizes the weights to preserve compactness:

$$\arg\min_{\hat{W}_{ei}} \|Z_i \hat{W}_{ei} - \mathbf{X}\|_2^2 + \lambda \|\hat{W}_{ei}\| \tag{2}$$

The concatenated feature array $Z^n \equiv [Z_1, \ldots, Z_n]$ forms the basis for constructing enhancement node groups H_m, which capture higher-order nonlinear dependencies. The final output aggregates all feature and enhancement activations, and the optimal terminal weight matrix W^m is computed through the Moore-Penrose pseudoinverse of the composite state matrix A^m. This single-step algebraic derivation replaces iterative backpropagation, facilitating rapid convergence on edge hardware.

2.2.2 Incremental Node Expansion

When the initial configuration lacks sufficient representational capacity, horizontal expansion is performed by appending additional nodes without discarding previously learned parameters [28, 29]. Concretely, upon appending a new enhancement node group, the augmented state matrix becomes $A^{m+1} = [A^m \mid \Delta H]$, where ΔH denotes the newly generated activation block. Rather than recomputing the pseudoinverse of the entire expanded matrix from scratch, a computationally efficient rank-one correction derives $(A^{m+1})^+$ directly from the prior state $(A^m)^+$, yielding an instantaneous terminal weight update that preserves all previously learned parameters. Feature node and corresponding enhancement node expansion proceeds analogously through block matrix inversion: the addition of a feature group ΔZ and its associated enhancement cluster triggers a synchronized weight adjustment via partitioned pseudoinverse recalculation. This differential weight computation is substantially cheaper than the full gradient-based retraining required by deep architectures, as its complexity scales with the width of the appended block rather than with the total network size.

Algorithm 1 Training and Inference of TABLNet

Require: Training data $\mathbf{X}_{train}$, labels $\mathbf{Y}_{train}$; test data $\mathbf{X}_{test}$; hyperparameters $n, m, k, \delta_x, \delta_u$.
Ensure: Predicted labels $\hat{\mathbf{Y}}_{test}$.

Phase 1: Initialization
Transform complex-valued I/Q data into real-valued vectors.
Generate initial feature nodes Z^n and enhancement nodes H^m.
Compute terminal weight matrix W^m via Moore-Penrose pseudoinverse.
Phase 2: Autonomous Structural Expansion
while feature expansion step $x_{et} > \delta_x$ **do**
    Update weights via block matrix inversion; evaluate a_{et+1}.
    if $a_{et+1} < a_{et}$ **then**
        Rollback; $x_{et} \leftarrow x_{et}/2$.
    end if
end while
while enhancement expansion step $u_{st} > \delta_u$ **do**
    Update weights via block matrix inversion; evaluate a_{st+1}.
    if $a_{st+1} < a_{st}$ **then**
        Rollback; $u_{st} \leftarrow u_{st}/2$.
    end if
end while
Phase 3: Inference
Propagate $\mathbf{X}_{test}$ through the optimized ABL network.
return $\hat{\mathbf{Y}}_{test}$.

2.2.3 Autonomous Width Calibration

To eliminate the overhead of manual trial-and-error hyperparameter selection, an autonomous calibration strategy constrains the network scale within an optimal operating zone [31]. A self-regulating loop monitors validation accuracy during each expansion cycle: if appending feature nodes causes performance degradation ($a_{et+1} < a_{et}$), the system reverts to the prior configuration and halves the expansion step. Conversely, when accuracy improves, lateral expansion persists. Iteration terminates once the step size falls below a preset threshold δ_x. A secondary refinement phase similarly optimizes the enhancement node count. Algorithm 1 formalizes the complete procedure.

3 Experimental Evaluation

3.1 Experimental Configuration

The practical deployment viability of the TABLNet framework is assessed through experiments on two publicly available RF signal repositories: the ADS-B dataset [32] and the XSRP dataset [33]. Hardware acceleration is provided by an NVIDIA Quadro RTX5000 GPU within a Keras-based computing environment.

Table 1 Hyperparameter Configuration

Hyperparameter	Value
Category count C	$\{10, 20, 30, 40, 50\}$
SNR range	$\{-5, 0, 5, 10, 15, 20\}$ dB
Initial feature nodes n	$10 \times C$
Initial enhancement nodes m	1 000
Feature expansion step x_1	C
Enhancement per feature k	10
Enhancement expansion step u_1	1 000
Threshold δ_x / δ_u	5 / 100

ADS-B Dataset: Electromagnetic emissions from aircraft transponders are captured using an SM200B software-defined radio receiver. Classification complexities range from 10 to 50 emitter categories, with 200 recordings per category and 4 800 digitized points per recording.

XSRP Dataset: Transmissions from 10 independent generators are collected under diverse line-of-sight (LoS) and non-line-of-sight (NLoS) propagation conditions. Each device is represented by 400 instances at a sample density of 30 720 points each.

Four deep learning architectures (LightAMC [27], DSN [24], MSCNN [25], CNN [34]) and two conventional signal-processing methods (HHT [35], CSI [11]) constitute the benchmark suite. Recognition accuracy and training duration serve as the principal evaluation metrics. Structural hyperparameters are specified in Table 1.

3.2 Performance Comparison on ADS-B Dataset

Classification accuracy and training latency across varying emitter category counts on the ADS-B benchmark are presented in Tables 2 and 3. The TABLNet framework attains the highest recognition rate in the majority of configurations. Although the MSCNN architecture exhibits a marginal precision advantage in the 10-class scenario, the proposed method demonstrates stronger resilience as classification complexity escalates. In particular, for the 50-category setting, competing models decline below 90% accuracy whereas TABLNet sustains a 91.23% recognition floor—a stability attributable to the autonomous node expansion that scales the generative topology in response to task difficulty. It is also noteworthy that traditional feature-engineering methods (HHT and CSI) suffer steep accuracy erosion as the number of target emitters increases, with CSI dropping from 66.03% at 10 categories to 50.60% at 50 categories, confirming that handcrafted transformations lack the capacity to discriminate among large emitter populations.

The computational advantage of TABLNet is pronounced. Model optimization for 10 to 50 emitter categories is accomplished within 5.16 to 50.05 seconds—an order-of-magnitude reduction compared with backpropagation-dependent baselines. For example, MSCNN requires 312.42 s for 10 categories and 1316.35 s for 50 categories, representing a 60× and 26× slowdown relative to TABLNet, respectively. Even among neural methods with relatively low overhead, LightAMC still consumes

Table 2 Accuracy (%) on the ADS-B Dataset

Method	10	20	30	40	50
HHT	63.52	58.14	54.36	53.28	44.42
CSI	66.03	62.52	58.49	54.14	50.60
DSN	97.86	91.49	91.57	82.93	80.92
CNN	92.89	90.18	89.30	84.50	81.60
MSCNN	**98.57**	95.80	94.91	93.51	86.12
LightAMC	95.49	92.57	91.89	91.20	85.16
TABLNet	98.34	**96.52**	**96.50**	**96.07**	**91.23**

Table 3 Training Time (s) on the ADS-B Dataset

Method	10	20	30	40	50
HHT	66.80	203.77	318.85	354.72	574.71
CSI	603.64	1140.81	1464.28	1649.84	2099.27
DSN	62.27	220.41	375.66	365.87	481.64
CNN	61.21	161.80	171.25	203.83	315.41
MSCNN	312.42	394.70	719.28	675.87	1316.35
LightAMC	39.95	66.08	97.99	119.36	152.48
TABLNet	**5.16**	**27.47**	**27.67**	**18.61**	**50.05**

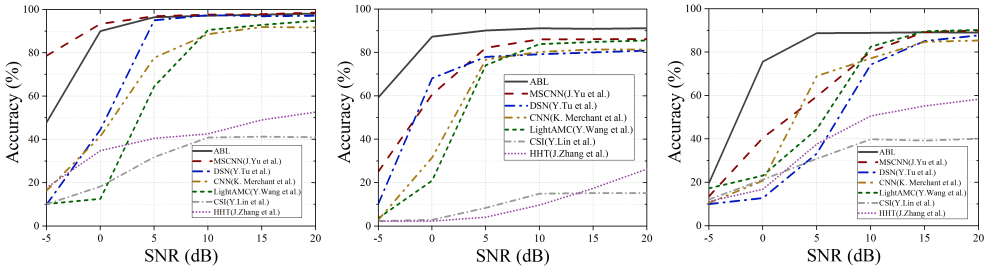
3× to 8× more time depending on task scale. This acceleration arises from the pseudoinverse-based weight derivation, which circumvents the iterative convergence cycles of gradient descent. The latency disparity widens as the category count grows, rendering conventional deep models impractical for real-time edge training.

3.3 Performance Comparison on XSRP Dataset

Comparative results on the XSRP benchmark appear in Table 4. TABLNet yields a slight accuracy deficit relative to DSN and MSCNN, a gap attributable to the elevated redundancy and noise floor of the dense XSRP sequences—each instance contains 30 720 sampling points, over six times the density of ADS-B recordings—that are more effectively denoised by deep hierarchical layers. Despite this marginal accuracy gap of approximately 1.2%, the 31.59-second training cycle of TABLNet is roughly 12× faster than LightAMC and over 30× faster than MSCNN, markedly outpacing every baseline. This trade-off strongly favors TABLNet in latency-sensitive IoT authentication scenarios where rapid model retraining upon device re-enrollment or environmental drift is critical.

Table 4 Performance on the XSRP Dataset

Method	Accuracy (%)	Training Time (s)
HHT	71.21	3427.83
CSI	74.64	3743.27
DSN	90.56	993.58
CNN	86.50	825.01
MSCNN	**91.03**	1197.14
LightAMC	90.17	372.11
TABLNet	89.79	**31.59**



(a) ADS-B, C=10 (b) ADS-B, C=50 (c) XSRP, C=10

Fig. 2 Recognition accuracy versus SNR under additive white Gaussian noise. (a) Low-complexity ADS-B scenario; (b) High-complexity ADS-B scenario; (c) XSRP cross-dataset evaluation.

3.4 Network Topology Sensitivity

The interplay between feature and enhancement node densities governs the representational efficacy of the ABL network. To investigate this relationship, parametric sweeps are conducted on the ADS-B dataset by varying feature node counts from 100 to 400 while keeping enhancement nodes fixed at 5 000, and vice versa.

Computational overhead scales approximately linearly with the number of feature nodes, while peak accuracy is attained at task-specific node densities. For 10 emitter categories, optimal accuracy (98.38%) is reached at 150 feature nodes with a training time of 5.23 s. As the number of categories grows, the optimal feature width shifts upward: 200 nodes for 20 categories (96.17%), 350 for 30 categories (95.71%), and 400 for both 40 and 50 categories (94.95% and 89.22%, respectively). Insufficient feature mapping leads to under-fitting, whereas excessive width introduces redundant parameters that degrade generalization. This trend underscores that classification complexity directly dictates the required generative capacity of the feature layer.

Conversely, expanding the enhancement layer beyond a critical mass yields diminishing returns. With 200 feature nodes held constant, increasing enhancement nodes from 4 000 to 10 000 produces only marginal accuracy fluctuations (<1% for most configurations), while training time rises from approximately 5 s to over 14 s for the 10-category case. This observation indicates that a moderate number of nonlinear enhancement nodes suffices to capture the essential signal variance, and that excessive

enhancement modules may inject mathematical noise without proportional benefit. Similar topology sensitivity patterns are observed on the XSRP dataset, where 150 feature nodes paired with 6 000 enhancement nodes yield the best trade-off between recognition accuracy (89.59%) and training efficiency (33.59 s).

3.5 Noise Robustness Analysis

Robustness under channel impairment is assessed by injecting additive white Gaussian noise at SNR levels spanning -5 to 20 dB. As shown in Fig. 2, TABLNet concedes accuracy primacy only to MSCNN below 5 dB. Above this threshold, the proposed framework consistently surpasses all baselines. At 0 dB, an 80% recognition floor is sustained, whereas deep architectures suffer pronounced degradation under combined high-noise and high-class-count conditions. Furthermore, TABLNet attains near-saturation accuracy above 5 dB, while MSCNN requires over 15 dB to stabilize in the 40-category task. On the XSRP benchmark, TABLNet achieves the highest recognition rate for all SNR levels below 15 dB, maintaining approximately 90% accuracy at 5 dB—in contrast to the sub-70% degradation exhibited by all competing methods. A marginal deficit relative to MSCNN and LightAMC emerges exclusively under high-fidelity conditions (SNR $\geq$ 15 dB). These observations confirm the superior noise resilience of the broad learning architecture.

4 Conclusion

This work introduces a trustworthy SEI framework grounded in adaptive broad learning to address the computational and latency constraints of edge-deployed IoT authentication systems. The TABLNet architecture supports high-precision end-to-end emitter discrimination while incorporating an autonomous structural scaling protocol that eliminates the reliance on iterative gradient optimization. By substituting backpropagation with pseudoinverse computation, the framework provides a practical foundation for low-power, rapidly trainable authentication on resource-limited IoT platforms. Experimental evaluations on two hardware-captured RF datasets with distinct signal densities and propagation conditions confirm the competitive accuracy and substantial training efficiency of TABLNet relative to established deep learning baselines, with training latency reduced by over an order of magnitude. Additionally, noise robustness experiments demonstrate that the flat-topology architecture maintains stable recognition performance under moderate-to-high channel interference, a property critical for real-world wireless environments.

Despite these promising results, certain limitations remain. The supervised nature of the current framework requires annotated training data, which may be unavailable in non-cooperative identification scenarios. Moreover, extremely high-density signal inputs with significant redundancy can slightly limit the flat topology compared with deep hierarchical denoising. Future work will explore unsupervised and semi-supervised extensions to accommodate label-scarce scenarios, as well as sparse node geometries and input-adaptive feature selection to further enhance scalability and robustness in high-density signal environments.

References

[1] Wang, X., Yang, L.T., Wang, Y., Ren, L., Deen, M.J.: ADTT: A highly efficient distributed tensor-train decomposition method for IIoT big data. IEEE Transactions on Industrial Informatics **17**(3), 1573–1582 (2021)

[2] Li, X., Dong, F., Zhang, S., Guo, W.: A survey on deep learning techniques in wireless signal recognition. Wireless Communications and Mobile Computing **2019**, 1–12 (2019) https://doi.org/10.1109/TPAMI.2019.2938758

[3] Yu, K., Tan, L., Aloqaily, M., Yang, H., Jararweh, Y.: Blockchain-enhanced data sharing with traceable and direct revocation in IIoT. IEEE Transactions on Industrial Informatics **17**(11), 7669–7678 (2021) https://doi.org/10.1109/TII.2021.3049141

[4] Lu, Y., Li, J., Zhang, Y.: Privacy-preserving and pairing-free multirecipient certificateless encryption with keyword search for cloud-assisted IIoT. IEEE Internet of Things Journal **7**(4), 2553–2562 (2020) https://doi.org/10.1109/JIOT.2019.2943379

[5] Pal, S., Jadidi, Z.: Analysis of security issues and countermeasures for the Industrial Internet of Things. Applied Sciences **11**(20) (2021) https://doi.org/10.3390/app11209393

[6] Qi, H., Wang, J., Li, W., Wang, Y., Qiu, T.: A blockchain-driven IIoT traffic classification service for edge computing. IEEE Internet of Things Journal **8**(4), 2124–2134 (2021) https://doi.org/10.1109/JIOT.2020.3035431

[7] Conoscenti, M., Vetrò, A., De Martin, J.C.: Blockchain for the Internet of Things: A systematic literature review. In: 2016 IEEE/ACS 13th International Conference of Computer Systems and Applications (AICCSA), pp. 1–6 (2017). https://doi.org/10.1109/AICCSA.2016.7945805

[8] He, B., Wang, F.: Cooperative specific emitter identification via multiple distorted receivers. IEEE Transactions on Information Forensics and Security **15**, 3791–3806 (2020)

[9] Wang, Y., Gui, G., Gacanin, H., Ohtsuki, T., Dobre, O.A., Poor, H.V.: An efficient specific emitter identification method based on complex-valued neural networks and network compression. IEEE Journal on Selected Areas in Communications **39**(8), 2305–2317 (2021) https://doi.org/10.1109/JSAC.2021.3087243

[10] Roy, D., Mukherjee, T., Chatterjee, M., Blasch, E., Pasiliao, E.: RFAL: Adversarial learning for RF transmitter identification and classification. IEEE Transactions on Cognitive Communications and Networking **6**(2), 783–801 (2020) https://doi.org/10.1109/TCCN.2019.2948919

[11] Lin, Y., Tu, Y., Dou, Z., Chen, L., Mao, S.: Contour stella image and deep learning for signal recognition in the physical layer. IEEE Transactions on Cognitive Communications and Networking **7**(1), 34–46 (2021) https://doi.org/10.1109/TCCN.2020.3024610

[12] Dong, Y., Jiang, X., Zhou, H., Lin, Y., Shi, Q.: SR2CNN: Zero-shot learning for signal recognition. IEEE Transactions on Signal Processing **69**, 2316–2329 (2021) https://doi.org/10.1109/TSP.2021.3070186

[13] Polak, A.C., Goeckel, D.L.: Identification of wireless devices of users who actively fake their RF fingerprints with artificial data distortion. IEEE Transactions on Wireless Communications **14**(11), 5889–5899 (2015) https://doi.org/10.1109/TWC.2015.2443794

[14] Zhang, Z., Guo, X., Lin, Y.: Trust management method of D2D communication based on RF fingerprint identification. IEEE Access **6**, 66082–66087 (2018) https://doi.org/10.1109/ACCESS.2018.2878595

[15] Xing, Y., Hu, A., Zhang, J., Yu, J., Li, G., Wang, T.: Design of a robust radio-frequency fingerprint identification scheme for multimode LFM radar. IEEE Internet of Things Journal **7**(10), 10581–10593 (2020) https://doi.org/10.1109/JIOT.2020.3003692

[16] Guo, S., Akhtar, S., Mella, A.: A method for radar model identification using time-domain transient signals. IEEE Transactions on Aerospace and Electronic Systems **57**(5), 3132–3149 (2021) https://doi.org/10.1109/TAES.2021.3074129

[17] Xie, R., Xu, W., Chen, Y., Yu, J., Hu, A., Ng, D.W.K., Swindlehurst, A.L.: A generalizable model-and-data driven approach for open-set RFF authentication. IEEE Transactions on Information Forensics and Security **16**, 4435–4450 (2021) https://doi.org/10.1109/TIFS.2021.3106166

[18] Wang, Y., Liu, M., Yang, J., Gui, G.: Data-driven deep learning for automatic modulation recognition in cognitive radios. IEEE Transactions on Vehicular Technology **68**(4), 4074–4077 (2019) https://doi.org/10.1109/TVT.2019.2900460

[19] Otter, D.W., Medina, J.R., Kalita, J.K.: A survey of the usages of deep learning for natural language processing. IEEE Transactions on Neural Networks and Learning Systems **32**(2), 604–624 (2021) https://doi.org/10.1109/TNNLS.2020.2979670

[20] Peng, L., Zhang, J., Liu, M., Hu, A.: Deep learning based RF fingerprint identification using differential constellation trace figure. IEEE Transactions on Vehicular Technology **69**(1), 1091–1095 (2020) https://doi.org/10.1109/TVT.2019.2950670

[21] Qian, Y., Qi, J., Kuai, X., Han, G., Sun, H., Hong, S.: Specific emitter identification based on multi-level sparse representation in automatic identification system.

IEEE Transactions on Information Forensics and Security **16**, 2872–2884 (2021) https://doi.org/10.1109/TIFS.2021.3068010

[22] Gong, J., Xu, X., Lei, Y.: Unsupervised specific emitter identification method using radio-frequency fingerprint embedded InfoGAN. IEEE Transactions on Information Forensics and Security **15**, 2898–2913 (2020)

[23] Liu, Z.: Multi-feature fusion for specific emitter identification via deep ensemble learning. Digital Signal Processing **110**, 102939 (2021)

[24] Tu, Y., Lin, Y., Hou, C., Mao, S.: Complex-valued networks for automatic modulation classification. IEEE Transactions on Vehicular Technology **69**(9), 10085–10089 (2020)

[25] Yu, J., Hu, A., Li, G., Peng, L.: A robust RF fingerprinting approach using multisampling convolutional neural network. IEEE Internet of Things Journal **6**(4), 6786–6799 (2019) https://doi.org/10.1109/JIOT.2019.2911347

[26] Xu, X., Jiang, T., Gong, J., Xu, H., Qin, X.: WLAN interference signal recognition using an improved quadruple generative adversarial network. Digital Signal Processing **117**, 103188 (2021)

[27] Wang, Y., Yang, J., Liu, M., Gui, G.: LightAMC: Lightweight automatic modulation classification via deep learning and compressive sensing. IEEE Transactions on Vehicular Technology **69**(3), 3491–3495 (2020) https://doi.org/10.1109/TVT.2020.2971001

[28] Chen, C.L.P., Liu, Z.: Broad learning system: An effective and efficient incremental learning system without the need for deep architecture. IEEE Transactions on Neural Networks and Learning Systems **29**(1), 10–24 (2018) https://doi.org/10.1109/TNNLS.2017.2716952

[29] Pu, X., Li, C.: Online semisupervised broad learning system for industrial fault diagnosis. IEEE Transactions on Industrial Informatics **17**(10), 6644–6654 (2021) https://doi.org/10.1109/TII.2020.3048990

[30] Dong, S., Wang, P., Abbas, K.: A survey on deep learning and its applications. Computer Science Review **40**, 100379 (2021)

[31] Fu, Y., Cao, H., Chen, X.: Adaptive broad learning system for high-efficiency fault diagnosis of rotating machinery. IEEE Transactions on Instrumentation and Measurement **70**, 1–11 (2021) https://doi.org/10.1109/TIM.2021.3085940

[32] Tu, Y., Lin, Y., Zha, H., Zhang, J., Wang, Y., Gui, G., Mao, S.: Large-scale real-world radio signal recognition with deep learning. Chinese Journal of Aeronautics (2021. doi: https://doi.org/10.1016/j.cja.2021.08.016.) https://doi.org/10.1016/j.cja.2021.08.016

[33] Zhang, S., Zhang, Y., Sun, J., Gui, G., Lin, Y., Gacanin, H., Adachi, F.: A Real-World Radio Frequency Signal Dataset Based on LTE System and Variable Channels. arXiv (2022). https://doi.org/10.48550/ARXIV.2205.12577 . https://arxiv.org/abs/2205.12577

[34] Merchant, K., Revay, S., Stantchev, G., Nousain, B.: Deep learning for RF device fingerprinting in cognitive communication networks. IEEE Journal of Selected Topics in Signal Processing **12**(1), 160–167 (2018) https://doi.org/10.1109/JSTSP.2018.2796446

[35] Zhang, J., Wang, F., Dobre, O.A., Zhong, Z.: Specific emitter identification via hilbert–huang transform in single-hop and relaying scenarios. IEEE Transactions on Information Forensics and Security **11**(6), 1192–1205 (2016) https://doi.org/10.1109/TIFS.2016.2520908